Cooperative Catalytic Effect of ZrO$_2$ and α-Fe$_2$O$_3$ Nanoparticles on BiVO$_4$ Photoanodes for Enhanced Photoelectrochemical Water Splitting

Maged N. Shaddad,[b] Mohamed A. Ghanem,[b] Abdullah M. AlMayouf,[b] Sixto Gimenez,[b] Juan Bisquert,*[a, b] and Isaac Herraiz-Cardona*[a]

Photoelectrochemical water splitting with metal oxide semiconductors offers a cost-competitive alternative for the generation of solar fuels. Most of the materials studied so far suffer from poor charge-transfer kinetics at the semiconductor/liquid interface, making compulsory the use of catalytic layers to overcome the large overpotentials required for the water oxidation reaction. Herein, we report a very soft electrolytic synthesis deposition method, which allows remarkably enhanced water oxidation kinetics of BiVO$_4$ photoanodes by the sequential addition of Zr and Fe precursors. Upon a heat treatment cycle, these precursors are converted into monoclinic ZrO$_2$ and α-Fe$_2$O$_3$ nanoparticles, which mainly act as catalysts, leading to a five-fold increase of the water oxidation photocurrent of BiVO$_4$. This method provides a versatile platform that is easy to apply to different semiconductor materials, fully reproducible, and facile to scale-up on large area conductive substrates with attractive implications for technological deployment.

■■Minor change to title for purely formatting reasons. Change ok?■■ Photoelectrochemical (PEC) water splitting driven by sunlight constitutes an environmentally friendly technology to store energy in the covalent bonds of H$_2$.[1] To efficiently convert solar photons into such a chemical fuel, semiconducting materials capable of absorbing a large fraction of the solar spectrum, with an adequate band edge position, and low overpotentials to carry out the hydrogen and/or oxygen evolution reactions are required. In particular, intensive research efforts have been accomplished to develop competitive n-type semiconducting materials working as water splitting photoanodes, as the oxygen evolution reaction (OER) is both kinetically and thermodynamically more demanding,[2] and the material suffers from severe oxidizing conditions.

[a] J. Bisquert, I. Herraiz-Cardona
Institute of Advanced Materials (INAM)
Universitat Jaume I
12006 Castelló (Spain)
E-mail: bisquert@uji.es
iherraiz@uji.es

[b] M. N. Shaddad, M. A. Ghanem, A. M. AlMayouf, S. Gimenez, J. Bisquert
Department of Chemistry, Faculty of Science
King Saud University
Riyadh (Saudi Arabia)

Supporting Information and the ORCID identification number(s) for the author(s) of this article can be found under http://dx.doi.org/10.1002/cssc.201600890.

To achieve cost-competitive, efficient, and durable devices, the use of low-cost, earth-abundant, stable materials synthesized by easily up-scalable methods is essential. In this context, metal oxides, such as monoclinic BiVO$_4$ (m-BiVO$_4$)[3] and α-Fe$_2$O$_3$,[4] have been deeply investigated as candidate photoanode materials. Although both of them satisfy many of the requirements, their poor electronic properties yield low solar-to-fuel efficiencies, preventing their large-scale use in PEC systems at present. To overcome this problem, different strategies have been implemented, including ion doping,[3d, g, 4a, c, 5] nanostructuring,[3a, f, 4a, 6] surface modification with passivation layers or electrocatalysts,[3b, d, 5d, 7] and combinatorial synthesis.[8] For example, α-Fe$_2$O$_3$ photoanodes have been successfully doped with heteroatoms like Sn,[5a] Ti,[4c] Zr,[5b, c] Si,[4a] and Nb.[5d] In the case of monoclinic BiVO$_4$ (m-BiVO$_4$), ■■definition added.■■ there are two different sites susceptible to metal doping, that is, Bi^{3+} and V^{5+}. Whereas the replacement of V^{5+} sites by six valence metal ions, such as Mo and W,[3d, 5e, f] has been largely explored, there are very few studies on doping Bi^{3+} sites, and are generally limited to theoretical calculations.[9] Hf^{4+}, Zr^{4+}, and Sn^{4+}, with ion radius relatively similar to Bi^{+3}, are potential candidates to occupy Bi positions in the m-BiVO$_4$ crystal structure. Luo et al.[10] synthesized BiVO$_4$ photoanodes doped by Sn^{+4} in Bi^{+3} positions by means of a metal–organic decomposition (MOD) method. A practically negligible improvement in photocurrent was reported for the doped sample, which was attributed to the high formation energy and the relatively low solubility of Sn^{4+} impurity ions into the crystal lattice.

The functional properties of BiVO$_4$ and Fe$_2$O$_3$ have also been separately improved by means of heterostructuring strategies. For instance, the PEC performance of BiVO$_4$ has been largely increased when deposited on nanostructured WO$_3$ layers, owing to the synergistic interaction between the BiVO$_4$ (providing good light harvesting properties) and WO$_3$ (enhanced charge transport).[3f, 11] Other different host–guest semiconductor combinations have been successfully implemented and tested with remarkable results for water splitting, like Si/TiO$_2$/BiVO$_4$,[12] SnO$_2$/BiVO$_4$,[13] WO$_3$/Fe$_2$O$_3$,[14] and Si/Fe$_2$O$_3$.[15]

Nevertheless, to the best of our knowledge, the heterostructured Fe$_2$O$_3$/BiVO$_4$ system, which would entirely match the stability and low-cost requirements, has not been tested for solar water oxidation. There is only one recent work in literature reporting the decoration of BiVO$_4$ with Fe$_2$O$_3$ nanoparticles, where it is suggested that Fe$_2$O$_3$ acts as an efficient co-catalyst for the degradation of organic pollutants.[16] Although different Fe-based catalysts have been successfully employed to deco-

These are not the final page numbers! ↗↗

rate semiconductor photoanodes, such as FeOOH[7a] and Ni-FeO$_x$,[3a, 17] the use of α-Fe$_2$O$_3$ nanoparticles as OER catalyst has not been explored.

Herein, we report a very soft electrolytic synthesis deposition method that is fully reproducible and facile to scale-up on large area conductive substrates, which allows enhancing remarkably the water oxidation kinetics of BiVO$_4$ photoanodes by the sequential addition of Zr and Fe precursors.

BiVO$_4$ photoanodes were synthesized by means of the two-step method developed by Choi et al.,[3c] which consisted of Bi electrodeposition on a fluorine-doped tin oxide (FTO) ■■definition added.■■ substrate followed by drop casting ■■ok? ■■ the V precursor and annealing at 500 °C for 2 h. Different amounts of Zr$_2$Cl$_2$O were incorporated into the Bi^{3+} plating bath as the source of Zr. Subsequently, electrodeposition of Fe on the as-prepared BiVO$_4$ layers followed by annealing at 450 °C was carried out to obtain Fe$_2$O$_3$ nanoparticles. Different electrodeposition charges were tested, ranging from 1 to 32 mC cm^{-2}. After systematic optimization of the deposition process, a five-fold increase of the water oxidation photocurrent at 1.23 V versus RHE was obtained compared to the reference BiVO$_4$ system. Figure 1 illustrates the photoelectrochemical behavior of the reference Fe$_2$O$_3$ (A) and BiVO$_4$ (B) photoanodes together with the best modified BiVO$_4$ electrodes: BiVO$_4$-Zr (C), BiVO$_4$-Fe (D), and BiVO$_4$-Zr-Fe (E). The photocurrents at 1.23 V versus RHE for the different Zr and Fe additions are showed in Figure 1b and are used ■■ok?■■ to determine the optimum synthetic conditions reported in Figure 1a. Typical volcano plots for both Zr and Fe additions on top of the BiVO$_4$ surface were obtained. The best performance was obtained for 2.5 mole% Zr. Note that this concentration is referred to the Zr/Bi molar ratio added to the electrodeposition bath. On the other hand, 2 mC cm^{-2} of total charge deposition of Fe yielded the optimum results. Although the photocurrents reported in Figure 1 are lower compared to previous studies on BiVO$_4$ photoanodes,[3a,b,7a] the efficiency is remarkably enhanced by the Zr and Fe additions compared with the reference material. Additionally, the simplicity of the method described here to engineer surface modifications can be mimicked in more efficient systems. Figure 1c shows the j–V curves when a hole scavenger (1 M Na$_2$SO$_3$) was added to the solution. In general, all BiVO$_4$-based samples exhibit practically the same behavior for sulfite oxidation when surface recombination is negligible, with photocurrents slightly higher than reported for oxygen evolution. This strongly suggests that the improvement reported for the optimized BiVO$_4$-Zr-Fe photoanode is mainly connected to surface catalysis.

To more precisely determine the role of both additives (Zr and Fe) on the PEC behavior of the photoelectrodes, detailed structural and optical characterization was performed. First, XRD measurements of the metallic deposits were carried out (see Figure SI1 in the Supporting Information). The results show that as the Zr content increases, the intensity of the peak assigned for Bi at $2\theta = 27.5°$ diminishes, which indicates that Bi–Zr codeposition was successfully accomplished. In addition, SEM images of as-deposited metals (Figure SI2) show a progressive morphological evolution with increased Zr additions, from dendrite trunks and branches (pure Bi deposits) to more compact films. Figure 2a and b show the SEM micrographs of pristine BiVO$_4$ and BiVO$_4$-Zr, with the optimum Zr addition (2.5 mol%), illustrating that after the vanadate formation process, the microstructure of the samples considerably changes to smoother-edged dendrites, although a high surface area is maintained. Furthermore, it is remarkable the decrease of the nanoparticle size from approximately 500 nm for pristine BiVO$_4$ to 200 nm for the optimized BiVO$_4$-Zr electrode. This is consistent with the role of Zr as grain growth inhibitor as reported for different metallurgical synthetic processes.[18] Figure 2c shows the XRD diffractograms of BiVO$_4$-Zr samples for different Zr additions, perfectly matching the monoclinic scheelite BiVO$_4$ structure (CAS Number 00-014-0688). The intensity of the ($\bar{1}$21) ■■ok?■■ peak increases with the Zr concentration up to the optimum 2.5 mol%, and is practically unchanged with further Zr additions. Moreover, the peak position shifts toward higher 2θ values for the most Zr-rich samples. This clearly involves a degradation of the film integrity as
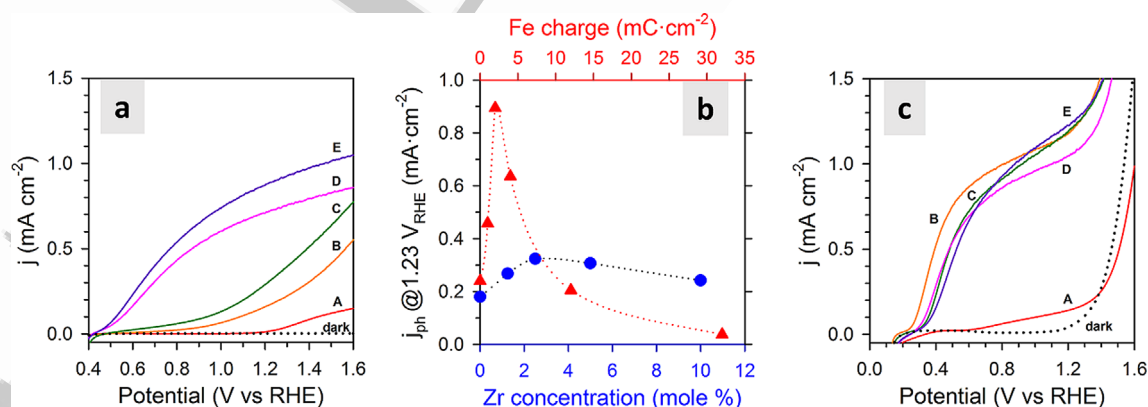

Figure 1. j–V curves of the synthetized films obtained in the dark (dashed lines) and under illumination at 100 mW cm^{-2} (solid lines) in phosphate buffer solution at pH 7.6 (a) without and (c) with a hole scavenger (1 M Na$_2$SO$_3$) in the solution. (b) Photocurrents obtained at 1.23 V vs. RHE for different Zr (blue symbols) and Fe (red symbols) additions in the phosphate buffer solution at pH 7.6. Labelled samples correspond to reference (A) α-Fe$_2$O$_3$ and (b) BiVO$_4$, and optimized (C) BiVO$_4$-Zr, (D) BiVO$_4$-Fe, and (E) BiVO$_4$-Zr-Fe photoanodes, respectively.

⬉⬉ These are not the final page numbers!
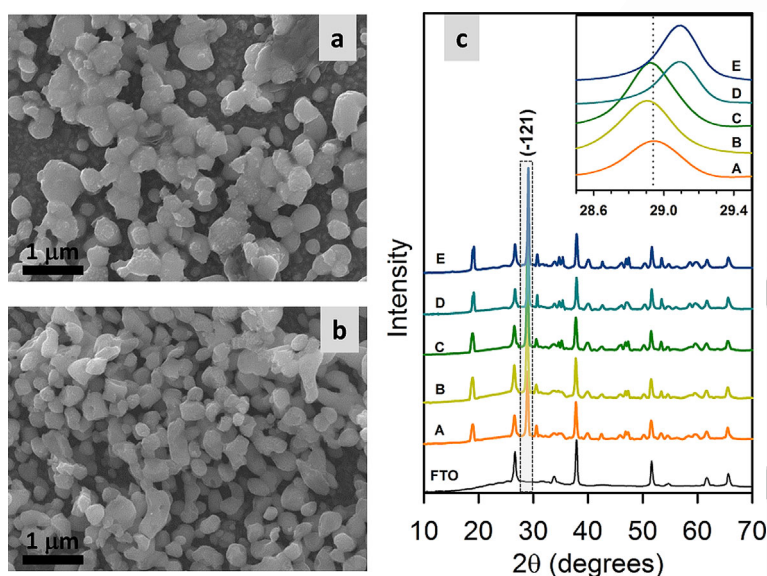
Figure 2. SEM images of (a) pristine and (b) after 2.5 mole% Zr addition to $BiVO_4$ films. (c) XRD patterns of pristine and modified $BiVO_4$ nanopowders with different Zr loadings. Labelled samples correspond to reference (A) $BiVO_4$ and (B) 1.25, (C) 2.5, (D) 5, and (E) 10% $BiVO_4$-Zr, respectively. The zoomed area shows the displacement of 2θ for the peak corresponding to the ($\bar{1}21$) ■■ok?■■ plane.

a result of the strain induced by the smaller ionic radius of Zr (0.79 Å) replacing Bi^{3+} positions (1.11 Å) into the periodic crystal lattice,[5g] which can be related to the progressive decrease of the photocurrent showed in Figure 1b for the higher Zr additions.

Figure 3 shows HR-TEM images of the optimized $BiVO_4$-Zr and $BiVO_4$-Zr-Fe photoanodes. The $BiVO_4$-Zr electrodes are
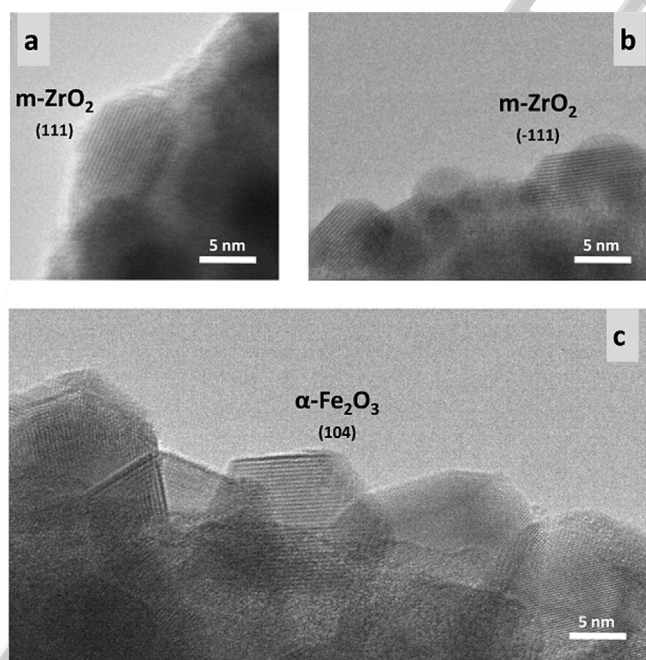
Figure 3. High resolution TEM images of optimized (a–b) $BiVO_4$-Zr photoanodes (2.5% Zr addition) and (c) $BiVO_4$-Zr-Fe electrodes (2.5 mole% Zr addition and electrodeposition of 2 mC cm^{-2} of Fe). In all images, lattice parameters were determined by the lattice fringes of the nanoparticles pointed by the arrows.

characterized by the presence of high crystalline nanoparticles (5–10 nm), with interplanar distances of 2.8 Å (Figure 3a) and 3.1 Å (Figure 3b) corresponding to the (111) and ($\bar{1}11$) reflections of monoclinic ZrO_2 (CAS Number 1309-37-1), respectively. Local energy dispersive X-ray spectroscopy (EDS) ■■definition added.■■ analyses confirmed the presence of Zr at these locations (Figure SI3), clearly indicating that although Zr can substitute Bi in the monoclinic $BiVO_4$ lattice as showed by XRD, an important fraction of Zr is present at the surface of $BiVO_4$ in the form of monoclinic ZrO_2 nanoparticles. The formation of ZrO_2 nanoparticles upon Zr addition has been reported even for low doping densities, below 1 at%.[19] On the other hand, the optimized $BiVO_4$-Zr-Fe samples, additionally showed the presence of crystalline nanoparticles, with interplanar distances of 2.7 Å (Figure 3c), corresponding to the (104) reflections of hexagonal scalenohedral α-Fe_2O_3, (CAS Number 1309-37-1) that appeared homogeneously dispersed on top of the $BiVO_4$-Zr photoanode.

The optical properties of $BiVO_4$ were not significantly altered by Zr additions, as showed in the Supporting Information (Figure SI4a), in good agreement with previous reports.[20] According to its bandgap of 2.4 eV, $BiVO_4$ is able to absorb light up to approximately 510 nm. On the other hand, as the amount of electrodeposited Fe increases, a broad shoulder appears on the 500–650 nm region, matching the main absorption band of α-Fe_2O_3 (Figure SI4b). A clear visual effect of the electrodeposition of different amounts of Fe can be observed in Figure SI5. At the highest Fe loading, the yellowish $BiVO_4$ substrate is completely covered and the samples have an orange/reddish color, characteristic of Fe_2O_3.

The estimated optical bandgaps (E_g) of the heterostructured materials were extracted from the Tauc plots for direct bandgap transitions (Figure SI4c). The obtained values are approximately 2.40 eV for pristine and $BiVO_4$-Zr samples, in good

These are not the final page numbers! ⌐⌐

agreement with those previously reported. A progressive decrease of the bandgap energy with the addition of Fe was detected, from an electrodeposition charge of 12 mC cm^{-2}, obtaining $E_g = 2.32$ eV for the highest Fe loading tested (i.e., 32 mC cm^{-2}), in good agreement with the optical properties of α-Fe$_2$O$_3$. From these optical absorption measurements, the maximum achievable photocurrent was calculated considering that all the photogenerated holes participate in the water oxidation reaction (j_{abs}), see Table SI1.

The enhanced PEC activity induced by the Zr and Fe additions was further corroborated by the incident photon-to-current efficiency (IPCE) spectra obtained at 1.23 V versus RHE without and with the addition of the hole scavenger (Figure 4a and b, respectively). There is an excellent correspondence between the onset wavelength of the IPCE and the absorbance measurements. Moreover, the integrated photocurrents extracted from the IPCE spectra nicely match those obtained from the j–V curves, as summarized in Table SI1. From the IPCE measurements in the solution with the hole scavenger, it is clear that the enhanced PEC behavior for the optimized heterostructure can be ascribed to the "cooperative" (rather than synergistic) catalytic effect of both ZrO$_2$ and α-Fe$_2$O$_3$ nanoparticles deposited on the top of the m-BiVO$_4$ films. Evidence of the excellent electrocatalytic behavior of α-Fe$_2$O$_3$ has been previously reported for Si photoanodes.[21] Conversely, nanostruc-

tured monoclinic ZrO$_2$ nanoparticles have demonstrated catalytic activity for different chemical reactions,[22] and has been also employed to passivate TiO$_2$ surface traps in dye-sensitized solar cells.[23] However, to the best of the authors knowledge it is the first time that they show enhanced water oxidation kinetics.

To quantitatively assess the beneficial effect of both Zr and Fe additions on BiVO$_4$ films, the charge separation (η_{cs}) and charge injection (η_{cat}) yields were calculated for the synthetized materials through Equations (1) and (2), by comparing the photocurrent for water splitting and to a hole scavenger:[24]

$$j_{H_2O} = j_{abs} \times \eta_{cs} \times \eta_{cat} \qquad (1)$$

$$j_{HS} = j_{abs} \times \eta_{cs} \qquad (2)$$

The comparative behavior of both calculated yields is showed in Figure 5. When Fe is distributed in the form of scattered Fe$_2$O$_3$ nanoparticles on the BiVO$_4$ surface, this material acts as an excellent catalyst for oxygen evolution reaction, doubling the catalytic efficiency of the semiconductor substrate. It is also remarkable the increase in the catalytic efficiency of BiVO$_4$-Zr samples, with respect to the reference BiVO$_4$. In contrast, the effect of Zr addition on the charge separation effi-
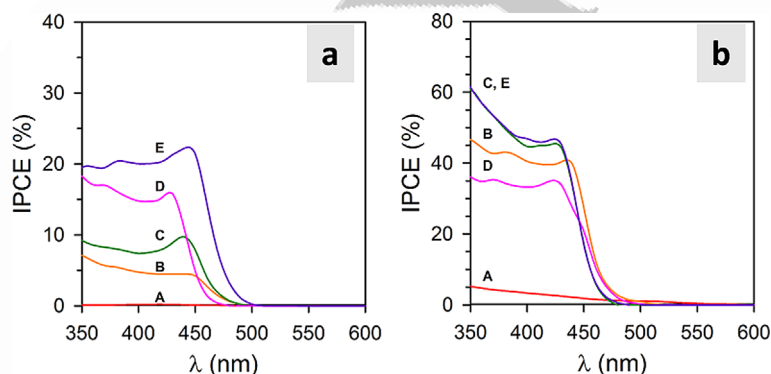
Figure 4. IPCE spectra obtained on the synthetized films at 1.23 V vs. RHE in phosphate buffer solution at pH 7.6 (a) without and (b) with hole scavenger (1 M Na$_2$SO$_3$). Labelled samples correspond to (A) α-Fe$_2$O$_3$, (B) reference BiVO$_4$, and optimized (C) BiVO$_4$-Zr, (D) BiVO$_4$-Fe, and (E) BiVO$_4$-Zr-Fe photoanodes, respectively.
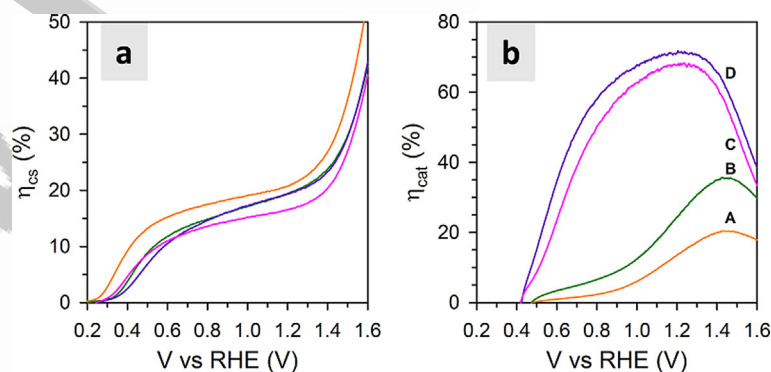
Figure 5. (a) Charge-separation efficiency and (b) charge-injection efficiency obtained on the synthesized films. Labelled samples correspond to (A) reference BiVO$_4$ and optimized (B) BiVO$_4$-Zr, (C) BiVO$_4$-Fe, and (D) BiVO$_4$-Zr-Fe samples, respectively.

↖↖ These are not the final page numbers!

ciency is negligible, in good agreement with previous reports suggesting that Zr additions on BiVO$_4$ do not affect the electronic properties of the material.[3e, 20] The validity of this analysis is based on the assumption of complete absence of surface recombination when the hole scavenger is employed. A marginal difference is observed in the measurements with the hole scavenger, which can be attributed to the role of ZrO$_2$ and α-Fe$_2$O$_3$ as surface passivation layers on top of BiVO$_4$.[7b] In any case, further analysis is needed to clarify this issue.

Figure SI6 shows the Mott–Schotky plots obtained in the dark on BiVO$_4$ and optimized BiVO$_4$-Zr and BiVO$_4$-Zr-Fe samples. The lower slope reported for the BiVO$_4$-Zr samples is connected to an increase in the surface area as shown in Figure 2, rather than to an increase in donor density. The material roughness is further increased for the BiVO$_4$-Zr-Fe sample, which can explain the lowest slope in the Mott–Schottky plot of Figure SI6, as a consequence of the Fe$_2$O$_3$ nanoparticle decoration and/or the ZrO$_2$ morphological rearrangement on top of BiVO$_4$ photoanode under the second annealing.[25] The calculated flat band potentials (V_{fb}) and donor densities (N_D) are collected in Table SI2. No significant changes are obtained for the electronic properties of BiVO$_4$ upon Zr and Fe additions, as reflected in the charge separation yield in Figure 5 a.

To benchmark the cooperative catalytic Zr–Fe-based layer developed in the present study, we have compared the reported behavior with that obtained with a FeOOH catalyst. For this purpose, we have deposited a FeOOH layer on top of our BiVO$_4$ photoanode, according to the optimum synthesis conditions described by Seabold and Choi in Ref. [7a]. Figure SI7 shows both the photoelectrochemical and optical properties of both systems. Our BiVO$_4$-Zr-Fe photoanode clearly outperforms BiVO$_4$-FeOOH in terms of delivered photocurrent. Additionally, the absorbance of our catalytic layer is significantly lower, which is particularly beneficial for application in tandem architectures.

In summary, we have reported a facile method to enhance the PEC water oxidation behavior of BiVO$_4$ photoanodes by controlled additions of Zr and Fe precursors on the electrodeposition bath. A remarkable five-fold increase of the photocurrent is reported for the optimized BiVO$_4$-Zr-Fe photoanodes, which can be explained by the cooperative catalytic role of monoclinic ZrO$_2$ and α-Fe$_2$O$_3$ nanoparticles distributed on the surface of BiVO$_4$. Although we show by XRD analysis that Zr can also extrinsically dope BiVO$_4$ replacing Bi atoms, the effect on the intrinsic electronic properties of BiVO$_4$ is not beneficial for the optimum Zr addition. The findings of this study can also be easily extrapolated to enhance the PEC performance of different photoanode materials with low-cost catalytic materials like Fe$_2$O$_3$ and ZrO$_2$, obtained by a simple, fully reproducible, and up-scalable synthesis.

Acknowledgements

[1] M. G. Walter, E. L. Warren, J. R. McKone, S. W. Boettcher, Q. Mi, E. A. Santori, N. S. Lewis, *Chem. Rev.* **2010**, *110*, 6446 – 6473.

[2] J. Tang, J. R. Durrant, D. R. Klug, *J. Am. Chem. Soc.* **2008**, *130*, 13885 – 13891.

[3] a) Y. Kuang, Q. Jia, H. Nishiyama, T. Yamada, A. Kudo, K. Domen, *Adv. Energy Mater.* **2016**, *6*, 1501645; b) T. W. Kim, K.-S. Choi, *Science* **2014**, *343*, 990 – 994; c) D. Kang, Y. Park, J. C. Hill, K.-S. Choi, *J. Phys. Chem. Lett.* **2014**, *5*, 2994 – 2999; d) F. F. Abdi, N. Firet, R. van de Krol, *ChemCatChem* **2013**, *5*, 490 – 496; e) W. Luo, Z. Yang, Z. Li, J. Zhang, J. Liu, Z. Zhao, Z. Wang, S. Yan, T. Yu, Z. Zou, *Energy Environ. Sci.* **2011**, *4*, 4046 – 4051; f) X. Shi, Y. Choi, K. Zhang, J. Kwon, D. Y. Kim, J. K. Lee, S. H. Oh, J. K. Kim, J. H. Park, *Nat. Commun.* **2014**, *5*, 4775; g) F. F. Abdi, L. Han, A. H. M. Smets, M. Zeman, B. Dam, R. van de Krol, *Nat. Commun.* **2013**, *4*, 2195.

[4] a) A. Kay, I. Cesar, M. Grätzel, *J. Am. Chem. Soc.* **2006**, *128*, 15714 – 15721; b) C. Du, X. Yang, M. T. Mayer, H. Hoyt, J. Xie, G. McMahon, G. Bischoping, D. Wang, *Angew. Chem. Int. Ed.* **2013**, *52*, 12692 – 12695; *Angew. Chem.* **2013**, *125*, 12924 – 12927; c) O. Zandi, B. M. Klahr, T. W. Hamann, *Energy Environ. Sci.* **2013**, *6*, 634 – 642.

[5] a) C. D. Bohn, A. K. Agrawal, E. C. Walter, M. D. Vaudin, A. A. Herzing, P. M. Haney, A. A. Talin, V. A. Szalai, *J. Phys. Chem. C* **2012**, *116*, 15290 – 15296; b) S. Shen, *J. Mater. Res.* **2014**, *29*, 29 – 46; c) P. Kumar, P. Sharma, R. Shrivastav, S. Dass, V. R. Satsangi, *Int. J. Hydrogen Energy* **2011**, *36*, 2777 – 2784; d) L. Steier, I. Herraiz-Cardona, S. Gimenez, F. Fabregat-Santiago, J. Bisquert, S. D. Tilley, M. Grätzel, *Adv. Funct. Mater.* **2014**, *24*, 7681 – 7688; e) K. P. S. Parmar, H. J. Kang, A. Bist, P. Dua, J. S. Jang, J. S. Lee, *ChemSusChem* **2012**, *5*, 1926 – 1934; f) H. S. Park, K. E. Kweon, H. Ye, E. Paek, G. S. Hwang, A. J. Bard, *J. Phys. Chem. C* **2011**, *115*, 17870 – 17879; g) J. D. Bryan, D. R. Gamelin, *Prog. Inorg. Chem.* **2005**, *54*, 47 – 126.

[6] F. E. Osterloh, *Chem. Soc. Rev.* **2013**, *42*, 2294 – 2320.

[7] a) J. A. Seabold, K.-S. Choi, *J. Am. Chem. Soc.* **2012**, *134*, 2186 – 2192; b) Y. Ma, A. Kafizas, S. R. Pendlebury, F. Le Formal, J. R. Durrant, *Adv. Funct. Mater.* **2016**, 4951 – 4960; c) D. K. Zhong, S. Choi, D. R. Gamelin, *J. Am. Chem. Soc.* **2011**, *133*, 18370 – 18377.

[8] C. Jiang, R. Wang, B. A. Parkinson, *ACS Comb. Sci.* **2013**, *15*, 639 – 645.

[9] a) Z. Zhao, W. Luo, Z. Li, Z. Zou, *Phys. Lett. A* **2010**, *374*, 4919 – 4927; b) W.-J. Yin, S.-H. Wei, M. M. Al-Jassim, J. Turner, Y. Yan, *Phys. Rev. B* **2011**, *83*, 155102.

[10] W. Luo, J. Wang, X. Zhao, Z. Zhao, Z. Li, Z. Zou, *Phys. Chem. Chem. Phys.* **2013**, *15*, 1006 – 1013.

[11] a) X. Shi, I. Herraiz-Cardona, L. Bertoluzzi, P. Lopez-Varo, J. Bisquert, J. H. Park, S. Gimenez, *Phys. Chem. Chem. Phys.* **2016**, *18*, 9255 – 9261; b) I. Grigioni, K. G. Stamplecoskie, E. Selli, P. V. Kamat, *J. Phys. Chem. C* **2015**, *119*, 20792 – 20800.

[12] H. Jung, S. Y. Chae, C. Shin, B. K. Min, O.-S. Joo, Y. J. Hwang, *ACS Appl. Mater. Interfaces* **2015**, *7*, 5788 – 5796.

[13] P. Chatchai, Y. Murakami, S.-y. Kishioka, A. Y. Nosaka, Y. Nosaka, *Electrochem. Solid-State Lett.* **2008**, *11*, H160 – H163.

[14] K. Sivula, F. L. Formal, M. Grätzel, *Chem. Mater.* **2009**, *21*, 2862 – 2867.

[15] M. T. Mayer, Y. Lin, G. Yuan, D. Wang, *Acc. Chem. Res.* **2013**, *46*, 1558 – 1566.

[16] P. Cai, S.-M. Zhou, D.-K. Ma, S.-N. Liu, W. Chen, S.-M. Huang, *Nano-Micro Lett.* **2015**, *7*, 183 – 193.

[17] J. E. Thorne, S. Li, C. Du, G. Qin, D. Wang, *J. Phys. Chem. Lett.* **2015**, *6*, 4083 – 4088.

[18] a) K. He, T. N. Baker, *Mater. Sci. Eng. A* **1998**, 256, 111 – 119; b) P. Z. Zhao, T. Tsuchida, *Mater. Sci. Eng. A* **2009**, *499*, 78 – 82.

[19] L. Hoffart, U. Heider, L. Jorissen, R. A. Huggins, W. Witschel, *Solid State Ionics* **1994**, *72*, 195 – 198.

[20] Z. Y. Zhao, W. J. Luo, Z. S. Li, Z. G. Zou, *Phys. Lett. A* **2010**, *374*, 4919 – 4927■■duplicate of ref. 9. Please replace with another reference or delete and renumber the remaining references.■■.

[21] K. Jun, Y. S. Lee, T. Buonassisi, J. M. Jacobson, *Angew. Chem. Int. Ed.* **2012**, *51*, 423 – 427; *Angew. Chem.* **2012**, *124*, 438 – 442.

[22] T. Yamaguchi, *Catal. Today* **1994**, *20*, 199 – 217.

[23] T. C. Li, M. S. Góes, F. Fabregat-Santiago, J. Bisquert, P. R. Bueno, C. Prasittichai, J. T. Hupp, T. J. Marks, *J. Phys. Chem. C* **2009**, *113*, 18385–18390.

[24] H. Dotan, K. Sivula, M. Graetzel, A. Rothschild, S. C. Warren, *Energy Environ. Sci.* **2011**, *4*, 958–964.

[25] G. Carraro, C. Maccato, A. Gasparotto, K. Kaunisto, C. Sada, D. Barreca, *Plasma Processes Polym.* **2016**, *13*, 191–200.

COMMUNICATIONS

All the nano things: A combination of ZrO_2 and $\alpha\text{-}Fe_2O_3$ nanoparticles deposited on the surface of a $BiVO_4$ film forms a catalytic layer that dramatically enhances the properties of the photoanode for water splitting driven by visible sunlight. A fully reproducible and facile electrolytic synthesis deposition method, which allows remarkably increased performance, indicates attractive implications for technological deployment.

H₂O

h⁺

ZrO₂ and Fe₂O₃ nanoparticles
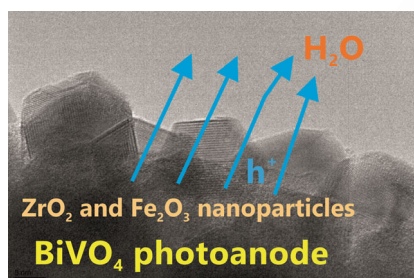
BiVO₄ photoanode

M. N. Shaddad, M. A. Ghanem,
A. M. AlMayouf, S. Gimenez, J. Bisquert,*
I. Herraiz-Cardona*

■■ – ■■

Cooperative Catalytic Effect of ZrO_2 and $\alpha\text{-}Fe_2O_3$ Nanoparticles on $BiVO_4$ Photoanodes for Enhanced Photoelectrochemical Water Splitting

---

Zr and Fe-based #nanoparticles deposited on BiVO4 #photoanodes lead to enhanced #watersplitting SPACE RESERVED FOR IMAGE AND LINK

Share your work on social media! *ChemSusChem* has added Twitter as a means to promote your article. Twitter is an online microblogging service that enables its users to send and read text-based messages of up to 140 characters, known as "tweets". Please check the pre-written tweet in the galley proofs for accuracy. Should you or your institute have a Twitter account, please let us know the appropriate username (i.e., @accountname), and we will do our best to include this information in the tweet. This tweet will be posted to the journal's Twitter account @ChemSusChem (follow us!) upon online publication of your article, and we recommended you to repost ("retweet") it to alert other researchers about your publication.

Please check that the ORCID identifiers listed below are correct. We encourage all authors to provide an ORCID identifier for each coauthor. ORCID is a registry that provides researchers with a unique digital identifier. Some funding agencies recommend or even require the inclusion of ORCID IDs in all published articles, and authors should consult their funding agency guidelines for details. Registration is easy and free; for further information, see http://orcid.org/.

Maged N. Shaddad
Mohamed A. Ghanem
Abdullah M. AlMayouf
Sixto Gimenez
Juan Bisquert http://orcid.org/0000-0003-4987-4887
Isaac Herraiz-Cardona

These are not the final page numbers! ↗↗